
Efficient Encoder-Decoder Transformer Decoding for Decomposable Tasks

Bo-Ru Lu [♣] Nikita Haduong [♣] Chien-Yu Lin [♣] Hao Cheng [♡]

Noah A. Smith ^{♣◇} Mari Ostendorf [♣]

[♣]University of Washington [♡]Microsoft Research [◇]Allen Institute for AI

roylu@u.washington.edu

Abstract

Transformer-based NLP models are powerful but have high computational costs that limit deployment. Finetuned encoder-decoder models are popular in specialized domains and can outperform larger more generalized decoder-only models, such as GPT-4. We introduce a new configuration for encoder-decoder models that improves efficiency on structured output and decomposable tasks where multiple outputs are required for a single shared input. Our method, *prompt-in-decoder* (PiD), encodes the input once and decodes the output in parallel, boosting both training and inference efficiency by avoiding duplicate input encoding and increasing the operational intensity (ratio of numbers of arithmetic operation to memory access) of decoding process by sharing the input key-value cache. We achieve computation reduction that roughly scales with the number of subtasks, gaining up to 4.6x speed-up over state-of-the-art models for dialogue state tracking, summarization, and question-answering tasks, with comparable or better performance.

1 Introduction

The transformer architecture [34] is the backbone of many successful NLP models, but they have high latency and computational costs. To reduce costs, researchers have investigated multiple approaches, including: i) model compression (e.g., distillation [12, 11, 33], quantization [45, 7, 38, 8, 48], and mixture of experts [16]); ii) decoding strategy (e.g., speculative decoding [19, 3] and parallel decoding [29, 25]); iii) algorithm-level attention optimizations (e.g., sparse attention [28, 22], fewer number of key-value heads [30, 1] and Hydragen [15]); iv) kernel-level attention optimizations (e.g., FlashAttention [5] and FlashInfer [42]); and v) memory management (e.g. paged attention[17] and radix attention [49]). Our work falls into the category of algorithm-level attention optimizations via key-value prefix sharing. We aim to upcycle existing encoder-decoder models with the goal of reducing redundant computations and increasing hardware utilization via key-value prefix sharing.

Recent research [35] indicates that scaling up decoder-only transformer models facilitates effective in-context learning, which is particularly beneficial when labeled data is scarce, making the models more generalized to unseen domains. However, these larger decoder-only models, despite their generalizability to unseen domains, incur higher computational costs and may offer inferior performance compared to smaller, specialized encoder-decoder transformer models [18]. Motivated by this, we propose a new configuration for encoder-decoder models to further improve training and inference efficiency in *decomposable* tasks that involve multiple prompts over the same document (or dialogue). These tasks include scenarios where multiple users are querying the same document with different requests (e.g., question answering, [43, 15]), as well as scenarios where it is useful to

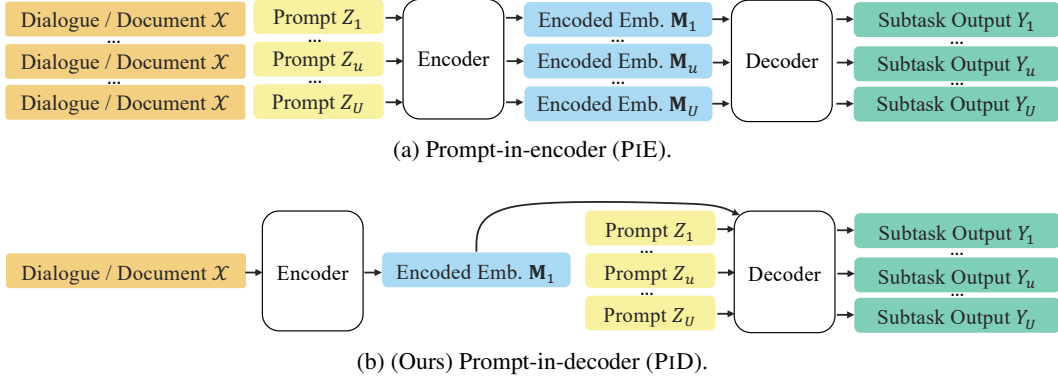


Figure 1: Given a task where a single input document \mathcal{X} is used to generate multiple outputs Y_u associated with different prompts Z_u , PIE creates unique encodings M_u for every prompt Z_u . In contrast, PID uses a single shared M for each prompt. thus requiring less memory access and resulting in higher computational efficiency.

decompose a complex task into simpler subtasks (e.g., abstractive summarization of long/multiple documents/dialogues [10, 24, 46, 44] and dialogue information extraction [23]).

In the multi-user question-answering scenario, decoupling questions and the corresponding document allows reusing the shared document embeddings for questions from different users. The shared embeddings can significantly reduce duplicate computation of the shared prefixes and increase operational intensity during training and inference. For summarization and information extraction, decomposing a long target output into multiple shorter sequences mitigates attention degeneration issues [9, 50], leading to a boost in accuracy and efficiency. However, existing methods put the prompts in the encoder, resulting in a high computation cost because contextualizing each shared document and its prompts results in the duplicate encoding of the same shared prefixes. Instead, we propose **prompt-in-decoder (PID)**: an encode-once, decode-in-parallel strategy that avoids duplicate encoding costs by sharing inputs and increases decoding efficiency by reducing memory access.

We demonstrate the effectiveness of our decoding strategy through experiments on a range of tasks with short and long inputs: dialogue state tracking, abstractive medical dialogue summarization, and extractive medical question answering. Our models achieve comparable or higher performance (98-101%) than the current state of the art. At the same time, we observe a 2-10x computation reduction, depending on the number of subtasks, and up to 4.6x speed-up for shorter subtask outputs. In summary, the main contribution of this work is a new, **more efficient decoding configuration for encoder-decoder models on decomposable tasks**, validated on multiple language tasks, including dialogue state tracking, medical summarization and question answering.

2 Encoder-Decoder Framework

The encoder-decoder is a general framework that has been used to address a wide variety of problems in NLP [20, 27]. Given an input word sequence, a desired result is obtained by first encoding the input and then iteratively generating an output word sequence. In general-purpose models, the input \mathcal{X} is optionally combined with a prompt \mathcal{Z} that specifies the task: $\mathcal{Y} = \text{decoder}(\text{encoder}(\mathcal{X}, \mathcal{Z}))$. The input \mathcal{X} is any form of text, e.g., a sentence, article, or transcript of a conversation, and \mathcal{Z} can be an instruction or a question. The output \mathcal{Y} could be information extracted from an article, a summary of a conversation, or a response to a question. State-of-the-art encoder-decoder systems are built on transformers. This section overviews the general framework to introduce notation and set up the multi-subtask inference problem that we address.

2.1 Multi-Prompt Decoding

In this paper, we tackle tasks that can be framed in terms of multiple prompts over the same input \mathcal{X} . Specifically, the output is a list of subtasks (or answers) \mathcal{Y} , where each subtask/answer is Y_u , e.g., $\mathcal{Y} = (Y_1, \dots, Y_u, \dots, Y_U)$, and U is the total number of subtasks/answers. Each subtask Y_u

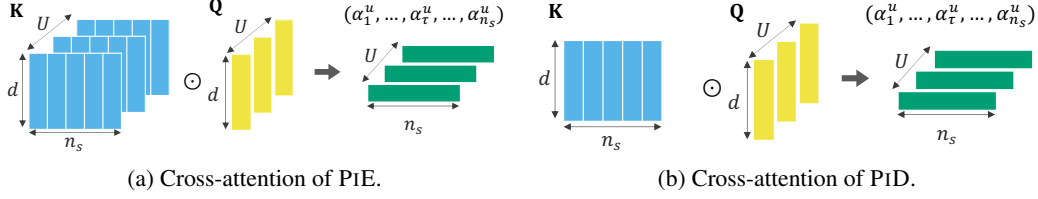


Figure 2: An illustration of cross-attention dot product operations ($\mathbf{Q}\mathbf{K}^\top$ in Equation 1) for PiE and PiD for a single inference step. U , d , n_s are the number of prompts, hidden layer dimension, and input length, respectively. \odot is the dot product operation, and the resulting scalars of $\mathbf{Q}\mathbf{K}^\top$ are α_τ^u , where $\tau = \{1, \dots, n_s\}$, at the decoding step τ w.r.t. the prompt Z_u .

is associated with a specific prompt Z_u , so $\mathcal{Z} = (Z_1, \dots, Z_u, \dots, Z_U)$. The scenario involves running inference multiple times to generate Y_u , $Y_u = \text{decoder}(\text{encoder}(\mathcal{X}, Z_u))$, then combining all outputs Y_u to form the final \mathcal{Y} . We refer to this as the **prompt-in-encoder (PiE)** approach. Figure 1(a) illustrates how PiE tackles a single instance $(\mathcal{X}, \mathcal{Y}$ and $\mathcal{Z})$. PiE involves U encodings of \mathcal{X} , one for each prompt Z_u .

2.2 Encode Once and Decode in Parallel

To avoid the redundant encoding of \mathcal{X} in PiE and improve inference efficiency when decoding Y_u , we propose placing prompt Z_u in the decoder, allowing us to encode \mathcal{X} once and decode Y_u in parallel. We refer to this method as **prompt-in-decoder (PiD)**. By moving Z_u from the encoder (in PiE) to the decoder, the encoder only encodes \mathcal{X} once, generating a single sequence of embeddings that is reused throughout the decoding process for each prompt Z_u . As shown in Figure 1(b), \mathcal{X} is only encoded once, and the embeddings \mathbf{M} are reused for U prompts during decoding to generate all subtask outputs $(Y_1, \dots, Y_u, \dots, Y_U)$. Formally, the equation can be represented as $Y_u = \text{decoder}(\text{encoder}(\mathcal{X}), Z_u)$.

3 Performance Analysis

In this section, we show how the PiD model improves inference efficiency over the PiE model by quantifying memory access and the number of arithmetic operations.

3.1 Operational Intensity

The operation intensity is the number of operations per byte of memory access, expressed as:

$$\text{Operational Intensity} = \frac{\text{FLOP/s}}{\text{byte/s}} = \frac{\# \text{ arithmetic operations}}{\text{memory access}},$$

which provides a measure for the hardware efficiency [36] or algorithm efficiency. To carry out calculations, accelerators must access and move data between global memory and registers, which can be a bottleneck because modern hardware accelerators such as GPUs/TPUs often have significantly greater capacity for computations compared to memory bandwidth. For example, an NVIDIA A100 GPU [4] has an operation capacity of 312 Tera FLOP/s versus a memory bandwidth of 2 Gigabyte/s. If the operational intensity is too low, the accelerator idles, waiting for data to move to registers instead of running computations. This often occurs in models where memory access is more intensive than arithmetic operations, i.e., incremental decoding in transformers [30]. By decreasing memory access, the operational intensity is increased, i.e., efficiency improves.

3.2 Multi-head Attention in Transformer

Transformers [34] have two types of multi-head attention: self-attention and cross-attention. Usually, the attention key and value tensors have the dimension d/h , where d is the dimension of input and output vectors and h is the number of attention heads. For simplicity, we consider the operations of all heads together such that the dimension of \mathbf{Q} , \mathbf{K} , \mathbf{V} (query/key/value) in the following section is denoted as d .

During attention, the query/key/value vectors can be obtained by projecting the corresponding input vectors $\mathbf{N} \in \mathbb{R}^{n \times d}$ or $\mathbf{M} \in \mathbb{R}^{m \times d}$, where n and m can be either n_s (input source length) or n_t (output target length). More formally, the equations are $\mathbf{Q} = \mathbf{N} \cdot W^Q \in \mathbb{R}^{n \times d}$, $\mathbf{K} = \mathbf{M} \cdot W^K \in \mathbb{R}^{m \times d}$ and $\mathbf{V} = \mathbf{M} \cdot W^V \in \mathbb{R}^{m \times d}$ where the projection matrices are $W^Q, W^K, W^V \in \mathbb{R}^{d \times d}$.

In the self-attention, \mathbf{N} is equivalent to \mathbf{M} ; hence, $m = n = n_s$ in the encoder or $m = n = n_t$ in the decoder. On the other hand, in the case of the cross-attention, the variable $\mathbf{N} \in \mathbb{R}^{n_t \times d}$ originates from the decoder, while $\mathbf{M} \in \mathbb{R}^{n_s \times d}$ is sourced from the output of the encoder.

The simplified equation of the attention mechanism is represented as follows,

$$\mathbf{O} = \text{softmax} \left(\frac{\mathbf{Q}\mathbf{K}^\top}{\sqrt{d/h}} \right) \mathbf{V} \cdot W^O, \quad (1)$$

where $\mathbf{O} \in \mathbb{R}^{m \times d}$ is the final attention output.

3.3 Performance Analysis for PiE and PiD

Figure 2 shows the dot product operation in the cross-attention for the two models. In the PiE model, the input is contextualized with each prompt, so the encoder’s output tensor differs for each prompt. Thus, at each decoding step τ , \mathbf{K} is read U times to generate U different sets of attention weights α_τ^u to decode Y_u . In contrast, in the PiD model, \mathbf{K} is shared across all prompts since the input is encoded independently of the prompts. Thus, at each decoding step τ , the dot product operation in the cross-attention shares and broadcasts \mathbf{K} and computes the dot product of \mathbf{K} and \mathbf{Q} , resulting in lower memory access but the same number of arithmetic operations compared to PiE.

We approximate the memory access and operations based on the dominant terms in the self- and cross-attention and ignore the constant terms. For a single input, the memory access of \mathbf{M} and \mathbf{N} is $n_s d$ and $n_t d$. The memory access of the matrices W^Q, W^K, W^V, W^O is d^2 . The number of operations in both attention mechanisms is dominated by the matrix projections which are used to obtain $\mathbf{Q}, \mathbf{K}, \mathbf{V}$, and \mathbf{O} ; thus, the number of operations is approximated as $n_s d^2$ or $n_t d^2$.

Table 1: Inference computation comparison between PiE and PiD, where U, b, n_s, n_t, d are the number of prompts, batch size, input source length, output target length, and hidden size, respectively.

Model	Encoder’s Self-attention		Decoder’s Self-attention		Decoder’s Cross-attention	
	Memory	Operations	Memory	Operations	Memory	Operations
PiE-T5	$Ubn_s d + d^2$	$Ubn_s d^2$	$Ubn_t^2 d + n_t d^2$	$Ubn_t d^2$	$Ubn_s n_t d + Ubn_t d + n_t d^2$	$Ubn_t d^2$
PiD-T5	$bn_s d + d^2$	$bn_s d^2$	$Ubn_t^2 d + n_t d^2$	$Ubn_t d^2$	$bn_s n_t d + Ubn_t d + n_t d^2$	$Ubn_t d^2$

The comparisons of memory access and operation counts on different inference components for our PiE and PiD implementations are presented in Table 1. The table demonstrates that PiD enhances efficiency by encoding only once and by boosting decoding efficiency through reduced memory access, achieved by sharing the input key-value cache. The count analysis is explained in further detail below. In the analysis, we assume that a batch of b inputs with the same set of U subtasks are processed together. The encoder input length and the decoder output length differ depending on whether the prompt is in the decoder. For simplicity, the analysis also assumes that the prompt terms are negligible; Appendix B provides the detailed justification.

Encoder’s self-attention. In PiE, to run inference on a single instance, the model encodes U prompts (Z_u) with input (\mathcal{X}). Considering a batch with b instances, PiE takes $Ubn_s d + d^2$ for memory access and $Ubn_s d^2$ for the number of operations. In contrast, PiD only encodes the input once, so the memory access and the number of operations remain $bn_s d + d^2$ and $bn_s d^2$. Thus, the encoders of both models have similar operational intensity, but PiE requires more memory access and more arithmetic computations.

Decoder’s self-attention. In both PiE and PiD, the decoder computes the self-attention for U prompts. For each decoding step, the memory access and the number of operations are $Ubn_t d$ and Ubd^2 . Thus, for n_t steps, the resulting memory access and the number of operations are $Ubn_t^2 d$ and $Ubn_t d^2$. In this case, PiE and PiD have roughly the same operational intensity.

Decoder’s cross-attention. Cross-attention dominates the inference cost. For each decoding step, we load the encoded input embeddings $\mathbf{M} \in \mathbb{R}^{m \times d}$, where $m = n_s$, from the encoder for each (\mathcal{X}, Z_u) input for PiE and \mathcal{X} for PiD. For PiE, the resulting b $(\mathbf{M}_1, \dots, \mathbf{M}_U)$ are fed into the decoder’s cross-attention for b instances with U prompts. On the other hand, PiD shares all \mathbf{M} for all U prompts of each instance, resulting in feeding b \mathbf{M} to the decoder. Therefore, for each step, the memory access for loading encoded \mathbf{M} is $Ubn_s d$ and $bn_s d$ for PiE and PiD, respectively. The memory access of loading \mathbf{Q} and \mathbf{O} is Ubd . Loading projection matrices takes d^2 . We multiply all memory access cost by a factor of n_t steps.

4 Datasets & Metrics

4.1 Datasets & Task Performance Metrics

Dialogue State Tracking (DST). Multi-domain Wizard-of-Oz dataset (MultiWoZ)[2] is a task-oriented dialogue dataset. We selected the most recent version of MultiWoZ 2.4 [40] due to its refined validation and test set annotations. For comparison to other work, joint goal accuracy (JGA) is adopted as the evaluation metric. The input \mathcal{X} is the dialogue history, \mathcal{Y} is the dialogue state, the subtask prompts Z_u are the domain-slot name, and the associated outputs Y_u are slot values.

Summarization. We use ACI-Bench [44], a dataset containing clinical notes associated with conversations between doctors and patients. The clinical notes have structured output with distinct sections. We use ROUGE-L score [21], denoted as R-L, to evaluate models. The input \mathcal{X} is the doctor-patient dialogue, \mathcal{Y} is the full clinical note, the subtask prompts Z_u are section indicators, and the associated outputs Y_u are section notes.

Question Answering. RadQA [31] is an extractive question-answering dataset on radiology reports with 3k questions posed by experts. A single report can have multiple questions. We use exact match (EM) as our evaluation metric. The input \mathcal{X} is the radiology report, the subtask prompts Z_u are specific questions, and the associated outputs Y_u are extracted responses.

4.2 Efficiency Metrics

Floating point operations (FLOPs) refer to the number of arithmetic operations required for model inference, i.e., the computational complexity.¹ Note that FLOP reduction may not correlate with wall-clock speed, as it tends to ignore overheads from memory access (IO) [5].

Latency. To account for extra IO costs, e.g., GPU memory bandwidth, we also report latency, which measures the wall clock time for a single instance inference in a single-user scenario (e.g., an edge computing device). Specifically, we report the average time for a single instance inference, where instances are processed sequentially.

Latency w/ Batching. For cloud-serving applications, multiple instances are computed in a batch fashion to fully utilize the computing device. We thus report the average time for a single instance, where a batch of instances is computed simultaneously.

To assess the FLOPs and latency, we randomly chose 512 samples from MultiWoZ 2.4 test set (due to the large test set) and used the full test sets for ACI-Bench and RadQA. We report the average latency and the average latency w/ batching at the optimal batch size.

5 Experiments & Results

5.1 Compared Systems

T5 [27] is adopted as the encoder-decoder model in all experiments. We use T5-base and T5-large models from HuggingFace for MultiWoZ 2.4 and ACI-Bench. For RadQA, we follow the previous work [18] and use a pretrained clinical T5. We denote base and large models in following tables as

¹We use calfllops [41] to compute FLOPs.

T5_{base} and T5_{large} (220M and 770M parameters respectively). We use T5 as the backbone to compare two different subtasking strategies: prompt-in-encoder (PiE) and our proposed prompt-in-decoder (PiD); thus the model size keeps the same as the standard T5.

LLaMA2 Touvron et al. [32] is a popular open decoder-only language model. Due to computation limitations, we adopt low-rank adaptation (LoRA) [13] to efficiently finetune LLaMA2 7B, resulting in approximately 80M trainable parameters with a rank of 64.

Current state-of-the-art models. We report the current best published results for in-context learning and full finetuning for every dataset. The source papers for the results of each dataset are documented in the caption of Table 4.

5.2 Training Procedure

The standard fine-tuned T5 and LLaMA2 data is represented as $(\mathcal{X}, \mathcal{Y})$, i.e. no prompts are used. For PiE-T5, the data is (\mathcal{X}, Y_u, Z_u) , since \mathcal{X} is separately contextualized with each subtask prompt Z_u and a subtask output Y_u , effectively increasing the dataset size by a factor of U and substantially extending the time required for training. In contrast, PiD-T5 has the flexibility to be trained using either data representation, as it uses shared inputs. We choose $(\mathcal{X}, \mathcal{Y}, \mathcal{Z})$ for PiD-T5 because it is more efficient to put all output \mathcal{Y} from the same shared input \mathcal{X} in the same batch to save encoding processing time during gradient update. The model selection criterion is the highest score on the validation set. Hyperparameters can be found in Appendix C.

5.3 Results

Task performance. Table 2 presents the task performance results for three different full finetuning scenarios (T5, PiE-T5, and PiD-T5), as well as a LoRA finetuned LLaMA2 language model. The results of MultiWoZ 2.4 and ACI-Bench indicate that subtasking and multi-prompt decoding help, since both PiE-T5 and PiD-T5 outperform the standard T5 and LLaMA2 models. Although larger model size often comes with better performance in moving from T5_{base} to T5_{large}, there are mixed results for LLaMA2 on these domains. One possible reason could be that the number of trainable parameters is fewer than that of full finetuning. More importantly, similar or greater gains in performance are obtained with smaller, more efficient models that leverage task structure.

Table 2: Task performance comparison between the baselines and PiD-T5 over the three test sets.

Model	MultiWoZ 2.4	ACI-Bench	RadQA
	JGA \uparrow	ROUGE-L \uparrow	EM \uparrow
T5 _{base}	71.5	47.9	–
PiE-T5 _{base}	76.3	53.8	53.7
PiD-T5 _{base}	75.5	54.0	52.4
T5 _{large}	72.5	52.5	–
PiE-T5 _{large}	77.5	54.7	55.4
PiD-T5 _{large}	76.5	55.2	54.6
LLaMA2 7B	66.1	53.8	54.4

Computation efficiency. Since PiE-T5 and PiD-T5 achieve better results than standard T5, we compare PiE-T5 and PiD-T5 in Table 3. Regarding computational efficiency, measured in FLOPs, PiD-T5 significantly outperforms PiE-T5 in reducing the number of arithmetic operations because it processes each input only once. PiD-T5 achieves superior speed-up in both single-instance and batching scenarios across three datasets and two model sizes, while obtaining similar performance (98-101%) to PiE-T5. Additionally, PiD-T5 offers greater reductions in computational costs (2-10x) and further accelerates efficiency when dealing with a larger number of subtasks—for example, managing 30 slots in MultiWoZ 2.4 versus 4 sections in ACI-Bench and 2-6 questions in RadQA.

Comparison between PiD-T5_{large} and state-of-the-art models. Table 4 illustrates the comparison between our method, PiD-T5_{large}, and existing state-of-the-art approaches. Our PiD-T5_{large}

Table 3: Task performance and inference efficiency comparison between PiE-T5, PiD-T5 and LLaMA2 over three test sets. Sp and Sp^{batch} represent the relative speed-up in single-instance and batching scenarios computed on NVIDIA A100. We present the relative ratios of FLOPs, Sp and Sp^{batch} compared to PiE-T5_{base} or PiE-T5_{large}, across other models. Overall, PiD-T5 achieves best computation efficiency across all tasks and achieves comparable task performance on MultiWoZ 2.4 and RadQA and better task performance on ACI-Bench.

Model	MultiWoZ 2.4				ACI-Bench				RadQA			
	JGA ↑	FLOPs ↓	Sp ↑	Sp ^{batch} ↑	R-L ↑	FLOPs ↓	Sp ↑	Sp ^{batch} ↑	EM ↑	FLOPs ↓	Sp ↑	Sp ^{batch} ↑
PiE-T5 _{base}	76.3	1.0x	1.0x	1.0x	53.8	1.0x	1.0x	1.0x	53.7	1.0x	1.0x	1.0x
PiD-T5 _{base}	75.5	0.1x	1.9x	4.6x	54.0	0.4x	1.1x	1.1x	52.4	0.6x	1.3x	1.3x
PiE-T5 _{large}	77.5	1.0x	1.0x	1.0x	54.7	1.0x	1.0x	1.0x	55.4	1.0x	1.0x	1.0x
PiD-T5 _{large}	76.5	0.1x	2.8x	4.2x	55.2	0.4x	1.0x	1.5x	54.6	0.5x	2.8x	1.3x
LLaMA2 _{7B}	66.1	0.7x	0.2x	0.5x	53.8	4.8x	0.3x	0.3x	54.4	26.8x	0.2x	0.1x

Table 4: We choose previous state-of-the-art (SOTA) generative models from the literature with the most comparable model sizes. In-context learning (ICL) SOTA results for MultiWoZ 2.4, ACI-Bench, and RadQA are reported in the studies [14, 44, 18]. For full finetuning (FT) SOTA, the results are reported in the studies [47, 44, 18]. Yim et al. [44] use four Bart_{large} models (one for each section), resulting in quadruple the size of a single Bart_{large} (406M). All numbers are reported on the test sets.

	MultiWoZ 2.4			ACI-Bench			RadQA		
	Model	Size ↓	JGA ↑	Model	Size ↓	R-L ↑	Model	Size ↓	EM ↑
ICL SOTA	Codex _{davinci}	175B	62.4	GPT4-32k	1760B	54.3	GPT3	175B	36.2
FT SOTA	T5 _{XXL}	11B	75.9	Bart _{large}	4×406M	48.6	T5 _{large}	770M	55.0
FT (Ours)	PiD-T5 _{large}	770M	76.5	PiD-T5 _{large}	770M	55.2	PiD-T5 _{large}	770M	54.6

outperforms in-context learning methods on all three datasets with much smaller models. Compared to full fine-tuning, our model outperforms on MultiWoZ 2.4 and ACI-Bench, but underperforms on RadQA. This discrepancy could be attributed to the fact that the prompts in RadQA are less structured compared to the fixed types of prompts in tasks with structured outputs.

We omit the inference cost of state-of-the-art models since access to the language models for in-context learning is restricted to API calls, and some finetuned models’ checkpoints are unavailable. Nevertheless, we can assume that the inference cost exceeds that of the proposed PiD-T5 due to the larger model sizes or inference techniques employed. The T5_{XXL} inference in MultiWoZ 2.4 follows the standard T5, while the inference approaches for Bart_{large} and T5_{large} in ACI-Bench and RadQA are consistent with those in PiE-T5.

Table 5: Comparison between in-context learning and full finetuning on MultiWoZ 2.4 test set. The JGA scores are reported at 1%, 5%, 10% and 100% of training data.

Models	Size	1%	5%	10%	100%
IC-DST (Codex-davinci)[14]	175B	48.4	55.4	56.9	62.4
PiD-T5 _{base} (ours)	220M	41.1	56.4	62.0	75.5

Comparison between in-context learning and finetuned models in the low-resource setting.

Table 5 shows the comparison between in-context learning and full finetuned models. We use the same 1%, 5% and 10% training set provided in Hu et al. [14]. PiD-T5_{base} surpasses Codex-davinci when the 5% training (≈ 374 examples) is available with 0.1% model size. The result suggests that the small, finetuned model is still useful when a reasonable amount of training data is available.

Training efficiency. Table 6 shows the training costs associated with models and training strategies described in subsection 5.2. Vanilla T5 may have longer sequences in a batch, whereas PiD-T5 breaks the sequence into smaller subtasks, reducing padding issues. PiE-T5_{base} incorporates prompts within its encoder, necessitating the enumeration of all prompts $\mathcal{Z} = (Z_1, \dots, Z_U)$ for every input \mathcal{X} during both training and testing phases. Consequently, PiE-T5_{base} requires more FLOPs, i.e., longer

Table 6: Comparison of training costs across models and the performance on MultiWoZ 2.4 test set.

	Data	Training FLOPs ↓	JGA on the test set ↑
T5 _{base}	(\mathcal{X}, \mathcal{Y})	1.5×10^{17}	71.5
PiE-T5 _{base}	(\mathcal{X}, Y_u, Z_u)	5.0×10^{18}	76.3
PiD-T5 _{base}	($\mathcal{X}, \mathcal{Y}, \mathcal{Z}$)	1.2×10^{17}	75.5

training duration, as the total number of training samples is increased by a factor of U . Conversely, PiD-T5_{base} allows the reuse of the same input across all prompts, keeping the total number of training examples the same as T5. PiD-T5_{base} not only maintains a comparable JGA score and has efficient inference but also reduces training costs.

Table 7: Comparison of latency (measured in msec) between different levels of GPUs on MultiWoZ 2.4 test set. L_{A100} and L_{2080Ti} stand for latency on NVIDIA A100 and RTX 2080Ti, respectively. Sp represent the relative speed-up relative to PiE-T5_{base} or PiD-T5_{large}.

	JGA ↑	L _{A100} ↓	Sp _{A100} ↑	L _{2080Ti} ↓	Sp _{2080Ti} ↑
PiE-T5 _{base}	76.3	146	1.0x	209	1.0x
PiD-T5 _{base}	75.5	78	1.9x	91	2.3x
PiE-T5 _{large}	77.5	413	1.0x	625	1.0x
PiD-T5 _{large}	76.5	147	2.8x	163	3.8x

Latency on different levels of GPUs. Table 7 illustrates that our PiD-T5_{base} surpasses PiE-T5_{base} in efficiency under a single-instance scenario. This difference becomes more pronounced when using a consumer-grade GPU, e.g., NVIDIA RTX 2080Ti, and inferecing on the larger model, showing PiD-T5 is more suitable when only lower resources are available.

Table 8: Comparison between different subtask scales, i.e., 30 domain slots or 5 domains, on MultiWoZ 2.4 test set. Sp represents the relative speed-up in latency computed on NVIDIA A100. The model with the domain subtask predicts all active slot values in that domain.

Model	Subtask	JGA ↑	FLOPs ↓	Sp ↑
T5 _{base}	All	71.5	1.0x	1.0x
PiD-T5 _{base}	Domain	72.5	2.3x	12.3x
PiD-T5 _{base}	Domain-Slot	75.5	2.5x	5.9x

Effect of different subtask granularity. In MultiWoZ 2.4, T5’s output can be broken down into subtasks according to either domains (where the output is a sequence of observed slots and their values) or domain-slot pairs (where the output is the slot value). Each domain or domain-slot pair is associated with a individual prompt. As demonstrated in Table 8, PiD-T5_{base} reveals that employing multi-prompt decoding can enhance both the inference speed and the JGA score, regardless of the granularity of the subtask units. While utilizing domains as subtask units leads to more speed-up, the use of slots as subtask units yields the best JGA.

Table 9: Comparison between T5, PiE-T5 and PiD-T5 on ACI-Bench test set.

Model	All	Section (ROUGE-L)			
		1	2	3	4
T5 _{base}	47.9	34.3	28.8	28.4	17.9
PiE-T5 _{base}	53.8	36.9	57.2	50.9	35.4
PiD-T5 _{base}	54.0	36.6	57.7	58.9	35.9

Effect of subtasking for long output. In ACI-Bench, We adopt the structure proposed by [44] for organizing the summary output into four distinct parts: subjective, objective examination, objective findings, and assessment with planning. The mean section output lengths are specified as 285, 98, 35, 254 tokens, respectively. The first section details the patient’s medical history, while the fourth section focuses on assessment and planning; these sections surpass the second and third sections in terms of length. Table 9 reveals that the standard T5_{base} model underperforms with longer outputs, especially when the generation reaches the end of the sequence, i.e., performance of later sections are much worse than for the other models. Both PiE-T5_{base} and PiD-T5_{base} models demonstrate improved performance with subtasking, allowing the model to “focus” on one subtask at a time.

6 Related Work

Improving the efficiency of transformer decoding hinges on minimizing memory access and reducing redundant computations via two primary ideas, increasing operational intensity and the reuse of key-value tensors. While most current research focuses on decoder-only models, our work emphasizes encoder-decoder models, as they offer superior performance in specialized domains.

Attention optimizations. Increasing operational intensity can be achieved through hardware-friendly attention functions or model architectures, which increase the number of operational operations per memory access. FlashAttention [5] and FlashInfer [42] use kernel-level optimization to fuse the attention mechanism into a single kernel function. Multi-query attention [30] and grouped-query attention [1] modify transformer architectures to employ a single (or fewer) key-value attention head for multiple query heads to reduce the memory access.

Key-value tensor caching. Another method to enhance decoding efficiency is the reuse of key-value tensors of shared common prefixes. This technique reduces redundant computations for subsequent requests with the same shared prefix. Methods like paged attention [17] and radix attention [49] mitigate the redundant storage of overlapping key-value cache. While paged attention and radix attention address the memory fragmentation issue and enable memory reuse for shared prefix, they remain less than optimally efficient because their implementation lacks compute-level memory optimization. Consequently, the key-value cache of the shared prefixes still needs to be loaded multiple times during computation.

Although most aforementioned methods focus on decoder-only models, our method is compatible with these kernel-level efficiency techniques, e.g., FlashAttention² and paged attention³, in principle leading to further efficiency gains when used in concert.

Hydragen [15] is the most closely related concurrent research to our work. Both our method and Hydragen aim to increase operational intensity by sharing key-value tensors for shared prefixes. However, Hydragen mainly focuses on decoder-only models and emphasizes speed-up metrics in question answering. In contrast, we focus on smaller encoder-decoder models, which can outperform larger decoder-only models in specialized in-domain tasks. We evaluate both speedup and accuracy metrics across various applications, including dialogue state tracking, summarization, and question answering.

7 Conclusion

We study settings for decomposable tasks in NLP where multiple subtask prompts are applied to the same document or dialogue. The subtasking approach allows an encoder-decoder model to individually address smaller and simpler components of the main task, leading to improved task performance. The strategy of moving the prompts from the encoder to the decoder allows our PiD configuration to reduce computational costs by encoding the input just once and then sharing it to multiple subtasks to decode outputs in parallel, which further speeds up inference time while either maintaining or improving task performance. Our approach achieves higher efficiency and comparable accuracy to existing approaches, which is particularly valuable in scenarios where computational resources are scarce.

²FlashT5 enhances T5 by incorporating FlashAttention. <https://github.com/catie-aq/flashT5>

³As of 05/22/2024, vLLM is planned to support encoder-decoder models but is still under development.

References

- [1] Joshua Ainslie, James Lee-Thorp, Michiel de Jong, Yury Zemlyanskiy, Federico Lebron, and Sumit Sanghai. GQA: Training generalized multi-query transformer models from multi-head checkpoints. In Houda Bouamor, Juan Pino, and Kalika Bali, editors, *Proceedings of the 2023 Conference on Empirical Methods in Natural Language Processing*, pages 4895–4901, Singapore, December 2023. Association for Computational Linguistics. doi: 10.18653/v1/2023.emnlp-main.298. URL <https://aclanthology.org/2023.emnlp-main.298>.
- [2] Paweł Budzianowski, Tsung-Hsien Wen, Bo-Hsiang Tseng, Iñigo Casanueva, Stefan Ultes, Osman Ramadan, and Milica Gašić. MultiWOZ - a large-scale multi-domain Wizard-of-Oz dataset for task-oriented dialogue modelling. In Ellen Riloff, David Chiang, Julia Hockenmaier, and Jun’ichi Tsujii, editors, *Proceedings of the 2018 Conference on Empirical Methods in Natural Language Processing*, pages 5016–5026, Brussels, Belgium, October–November 2018. Association for Computational Linguistics. doi: 10.18653/v1/D18-1547. URL <https://aclanthology.org/D18-1547>.
- [3] Charlie Chen, Sebastian Borgeaud, Geoffrey Irving, Jean-Baptiste Lespiau, Laurent Sifre, and John Jumper. Accelerating large language model decoding with speculative sampling. *arXiv preprint arXiv:2302.01318*, 2023. URL <https://arxiv.org/pdf/2302.01318>.
- [4] Jack Choquette, Wishwesh Gandhi, Olivier Giroux, Nick Stam, and Ronny Krashinsky. Nvidia a100 tensor core gpu: Performance and innovation. *IEEE Micro*, 41(2):29–35, 2021. URL <https://ieeexplore.ieee.org/document/9361255>.
- [5] Tri Dao, Daniel Y. Fu, Stefano Ermon, Atri Rudra, and Christopher Ré. FlashAttention: Fast and memory-efficient exact attention with IO-awareness. In *Advances in Neural Information Processing Systems*, 2022. URL https://proceedings.neurips.cc/paper_files/paper/2022/file/67d57c32e20fd0a7a302cb81d36e40d5-Paper-Conference.pdf.
- [6] Michiel de Jong, Yury Zemlyanskiy, Joshua Ainslie, Nicholas FitzGerald, Sumit Sanghai, Fei Sha, and William Cohen. FiDO: Fusion-in-decoder optimized for stronger performance and faster inference. In Anna Rogers, Jordan Boyd-Graber, and Naoaki Okazaki, editors, *Findings of the Association for Computational Linguistics: ACL 2023*, pages 11534–11547, Toronto, Canada, July 2023. Association for Computational Linguistics. doi: 10.18653/v1/2023.findings-acl.732. URL <https://aclanthology.org/2023.findings-acl.732>.
- [7] Tim Dettmers, Mike Lewis, Younes Belkada, and Luke Zettlemoyer. GPT3.int8(): 8-bit matrix multiplication for transformers at scale. In Alice H. Oh, Alekh Agarwal, Danielle Belgrave, and Kyunghyun Cho, editors, *Advances in Neural Information Processing Systems*, 2022. URL <https://openreview.net/forum?id=dXiGWqBoxaD>.
- [8] Tim Dettmers, Artidoro Pagnoni, Ari Holtzman, and Luke Zettlemoyer. QLoRA: Efficient finetuning of quantized LLMs. In *Thirty-seventh Conference on Neural Information Processing Systems*, 2023. URL <https://openreview.net/forum?id=OUIFPHEgJU>.
- [9] Zihao Fu, Wai Lam, Qian Yu, Anthony Man-Cho So, Shengding Hu, Zhiyuan Liu, and Nigel Collier. Decoder-only or encoder-decoder? interpreting language model as a regularized encoder-decoder. *arXiv preprint arXiv:2304.04052*, 2023. URL <https://arxiv.org/abs/2304.04052>.
- [10] Alexios Gidiotis and Grigorios Tsoumakas. A divide-and-conquer approach to the summarization of long documents. *IEEE/ACM Transactions on Audio, Speech, and Language Processing*, 28:3029–3040, 2020. URL <https://ieeexplore.ieee.org/document/9257174>.
- [11] Jianping Gou, Baosheng Yu, Stephen J Maybank, and Dacheng Tao. Knowledge distillation: A survey. *International Journal of Computer Vision*, 129:1789–1819, 2021. URL <https://arxiv.org/abs/2006.05525>.
- [12] Geoffrey Hinton, Oriol Vinyals, and Jeffrey Dean. Distilling the knowledge in a neural network. In *NIPS Deep Learning and Representation Learning Workshop*, 2015. URL <http://arxiv.org/abs/1503.02531>.

- [13] Edward J Hu, yelong shen, Phillip Wallis, Zeyuan Allen-Zhu, Yuanzhi Li, Shean Wang, Lu Wang, and Weizhu Chen. LoRA: Low-rank adaptation of large language models. In *International Conference on Learning Representations*, 2022. URL <https://openreview.net/forum?id=nZeVKeeFYf9>.
- [14] Yushi Hu, Chia-Hsuan Lee, Tianbao Xie, Tao Yu, Noah A. Smith, and Mari Ostendorf. In-context learning for few-shot dialogue state tracking. In Yoav Goldberg, Zornitsa Kozareva, and Yue Zhang, editors, *Findings of the Association for Computational Linguistics: EMNLP 2022*, pages 2627–2643, Abu Dhabi, United Arab Emirates, December 2022. Association for Computational Linguistics. doi: 10.18653/v1/2022.findings-emnlp.193. URL <https://aclanthology.org/2022.findings-emnlp.193>.
- [15] Jordan Juravsky, Bradley Brown, Ryan Ehrlich, Daniel Y Fu, Christopher Ré, and Azalia Mirhoseini. Hydragen: High-throughput llm inference with shared prefixes. *arXiv preprint arXiv:2402.05099*, 2024. URL <https://arxiv.org/abs/2402.05099>.
- [16] Sneha Kudugunta, Yanping Huang, Ankur Bapna, Maxim Krikun, Dmitry Lepikhin, Minh-Thang Luong, and Orhan Firat. Beyond distillation: Task-level mixture-of-experts for efficient inference. In Marie-Francine Moens, Xuanjing Huang, Lucia Specia, and Scott Wen-tau Yih, editors, *Findings of the Association for Computational Linguistics: EMNLP 2021*, pages 3577–3599, Punta Cana, Dominican Republic, November 2021. Association for Computational Linguistics. doi: 10.18653/v1/2021.findings-emnlp.304. URL <https://aclanthology.org/2021.findings-emnlp.304>.
- [17] Woosuk Kwon, Zhuohan Li, Siyuan Zhuang, Ying Sheng, Lianmin Zheng, Cody Hao Yu, Joseph Gonzalez, Hao Zhang, and Ion Stoica. Efficient memory management for large language model serving with pagedattention. In *Proceedings of the 29th Symposium on Operating Systems Principles*, pages 611–626, 2023. URL <https://dl.acm.org/doi/10.1145/3600006.3613165>.
- [18] Eric Lehman, Evan Hernandez, Diwakar Mahajan, Jonas Wulff, Micah J Smith, Zachary Ziegler, Daniel Nadler, Peter Szolovits, Alistair Johnson, and Emily Alsentzer. Do we still need clinical language models? In Bobak J. Mortazavi, Tasmie Sarker, Andrew Beam, and Joyce C. Ho, editors, *Proceedings of the Conference on Health, Inference, and Learning*, volume 209 of *Proceedings of Machine Learning Research*, pages 578–597. PMLR, 22 Jun–24 Jun 2023. URL <https://proceedings.mlr.press/v209/eric23a.html>.
- [19] Yaniv Leviathan, Matan Kalman, and Yossi Matias. Fast inference from transformers via speculative decoding. In *International Conference on Machine Learning*, pages 19274–19286. PMLR, 2023. URL <https://proceedings.mlr.press/v202/leviathan23a/leviathan23a.pdf>.
- [20] Mike Lewis, Yinhan Liu, Naman Goyal, Marjan Ghazvininejad, Abdelrahman Mohamed, Omer Levy, Veselin Stoyanov, and Luke Zettlemoyer. BART: Denoising sequence-to-sequence pre-training for natural language generation, translation, and comprehension. In Dan Jurafsky, Joyce Chai, Natalie Schluter, and Joel Tetreault, editors, *Proceedings of the 58th Annual Meeting of the Association for Computational Linguistics*, pages 7871–7880, Online, July 2020. Association for Computational Linguistics. doi: 10.18653/v1/2020.acl-main.703. URL <https://aclanthology.org/2020.acl-main.703>.
- [21] Chin-Yew Lin. ROUGE: A package for automatic evaluation of summaries. In *Text Summarization Branches Out*, pages 74–81, Barcelona, Spain, July 2004. Association for Computational Linguistics. URL <https://aclanthology.org/w04-1013>.
- [22] Liu Liu, Zheng Qu, Zhaodong Chen, Fengbin Tu, Yufei Ding, and Yuan Xie. Dynamic sparse attention for scalable transformer acceleration. *IEEE Transactions on Computers*, 71:3165–3178, 2022. URL <https://api.semanticscholar.org/CorpusID:252421345>.
- [23] Bo-Ru Lu, Nikita Haduong, Chia-Hsuan Lee, Zeqiu Wu, Hao Cheng, Paul Koester, Jean Utke, Tao Yu, Noah A Smith, and Mari Ostendorf. Does collaborative human-llm dialogue generation help information extraction from human dialogues? *arXiv preprint arXiv:2307.07047*, 2023. URL <https://arxiv.org/abs/2307.07047>.

- [24] Rui Meng, Khushboo Thaker, Lei Zhang, Yue Dong, Xingdi Yuan, Tong Wang, and Daqing He. Bringing structure into summaries: a faceted summarization dataset for long scientific documents. In Chengqing Zong, Fei Xia, Wenjie Li, and Roberto Navigli, editors, *Proceedings of the 59th Annual Meeting of the Association for Computational Linguistics and the 11th International Joint Conference on Natural Language Processing (Volume 2: Short Papers)*, pages 1080–1089, Online, August 2021. Association for Computational Linguistics. doi: 10.18653/v1/2021.acl-short.137. URL <https://aclanthology.org/2021.acl-short.137>.
- [25] Xuefei Ning, Zinan Lin, Zixuan Zhou, Zifu Wang, Huazhong Yang, and Yu Wang. Skeleton-of-thought: Prompting LLMs for efficient parallel generation. In *The Twelfth International Conference on Learning Representations*, 2024. URL <https://openreview.net/forum?id=mqVgBbNCm9>.
- [26] Adam Paszke, Sam Gross, Francisco Massa, Adam Lerer, James Bradbury, Gregory Chanan, Trevor Killeen, Zeming Lin, Natalia Gimelshein, Luca Antiga, et al. Pytorch: An imperative style, high-performance deep learning library. *Advances in neural information processing systems*, 32, 2019. URL https://proceedings.neurips.cc/paper_files/paper/2019/file/bdbca288fee7f92f2bfa9f7012727740-Paper.pdf.
- [27] Colin Raffel, Noam Shazeer, Adam Roberts, Katherine Lee, Sharan Narang, Michael Matena, Yanqi Zhou, Wei Li, and Peter J. Liu. Exploring the limits of transfer learning with a unified text-to-text transformer. *Journal of Machine Learning Research*, 21(140):1–67, 2020. URL <http://jmlr.org/papers/v21/20-074.html>.
- [28] Aurko Roy, Mohammad Saffar, Ashish Vaswani, and David Grangier. Efficient Content-Based Sparse Attention with Routing Transformers. *Transactions of the Association for Computational Linguistics*, 9:53–68, 02 2021. ISSN 2307-387X. doi: 10.1162/tacl_a_00353. URL https://doi.org/10.1162/tacl_a_00353.
- [29] Andrea Santilli, Silvio Severino, Emilian Postolache, Valentino Maiorca, Michele Mancusi, Riccardo Marin, and Emanuele Rodola. Accelerating transformer inference for translation via parallel decoding. In Anna Rogers, Jordan Boyd-Graber, and Naoaki Okazaki, editors, *Proceedings of the 61st Annual Meeting of the Association for Computational Linguistics (Volume 1: Long Papers)*, pages 12336–12355, Toronto, Canada, July 2023. Association for Computational Linguistics. doi: 10.18653/v1/2023.acl-long.689. URL <https://aclanthology.org/2023.acl-long.689>.
- [30] Noam Shazeer. Fast transformer decoding: One write-head is all you need. *arXiv preprint arXiv:1911.02150*, 2019. URL <https://arxiv.org/abs/1911.02150>.
- [31] Sarvesh Soni, Meghana Gudala, Atieh Pajouhi, and Kirk Roberts. RadQA: A question answering dataset to improve comprehension of radiology reports. In Nicoletta Calzolari, Frédéric B chet, Philippe Blache, Khalid Choukri, Christopher Cieri, Thierry Declerck, Sara Goggi, Hitoshi Isahara, Bente Maegaard, Joseph Mariani, H l ne Mazo, Jan Odijk, and Stelios Piperidis, editors, *Proceedings of the Thirteenth Language Resources and Evaluation Conference*, pages 6250–6259, Marseille, France, June 2022. European Language Resources Association. URL <https://aclanthology.org/2022.lrec-1.672>.
- [32] Hugo Touvron, Louis Martin, Kevin Stone, Peter Albert, Amjad Almahairi, Yasmine Babaei, Nikolay Bashlykov, Soumya Batra, Prajjwal Bhargava, Shruti Bhosale, et al. Llama 2: Open foundation and fine-tuned chat models. *arXiv preprint arXiv:2307.09288*, 2023. URL <https://arxiv.org/abs/2307.09288>.
- [33] Takuma Udagawa, Aashka Trivedi, Michele Merler, and Bishwaranjan Bhattacharjee. A comparative analysis of task-agnostic distillation methods for compressing transformer language models. In *Conference on Empirical Methods in Natural Language Processing*, 2023. URL <https://api.semanticscholar.org/CorpusID:264127930>.
- [34] Ashish Vaswani, Noam Shazeer, Niki Parmar, Jakob Uszkoreit, Llion Jones, Aidan N Gomez, Łukasz Kaiser, and Illia Polosukhin. Attention is all you need. *Advances in Neural Information Processing Systems*, 30, 2017. URL https://proceedings.neurips.cc/paper_files/paper/2017/file/3f5ee243547dee91fbd053c1c4a845aa-Paper.pdf.

- [35] Jason Wei, Yi Tay, Rishi Bommasani, Colin Raffel, Barret Zoph, Sebastian Borgeaud, Dani Yogatama, Maarten Bosma, Denny Zhou, Donald Metzler, Ed H. Chi, Tatsunori Hashimoto, Oriol Vinyals, Percy Liang, Jeff Dean, and William Fedus. Emergent abilities of large language models. *Transactions on Machine Learning Research*, 2022. ISSN 2835-8856. URL <https://openreview.net/forum?id=yzkSU5zdWd>. Survey Certification.
- [36] Samuel Williams, Andrew Waterman, and David Patterson. Roofline: an insightful visual performance model for multicore architectures. *Commun. ACM*, 52(4):65–76, apr 2009. ISSN 0001-0782. doi: 10.1145/1498765.1498785. URL <https://doi.org/10.1145/1498765.1498785>.
- [37] Thomas Wolf, Lysandre Debut, Victor Sanh, Julien Chaumond, Clement Delangue, Anthony Moi, Pierric Cistac, Tim Rault, Remi Louf, Morgan Funtowicz, Joe Davison, Sam Shleifer, Patrick von Platen, Clara Ma, Yacine Jernite, Julien Plu, Canwen Xu, Teven Le Scao, Sylvain Gugger, Mariama Drame, Quentin Lhoest, and Alexander Rush. Transformers: State-of-the-art natural language processing. In Qun Liu and David Schlangen, editors, *Proceedings of the 2020 Conference on Empirical Methods in Natural Language Processing: System Demonstrations*, pages 38–45, Online, October 2020. Association for Computational Linguistics. doi: 10.18653/v1/2020.emnlp-demos.6. URL <https://aclanthology.org/2020.emnlp-demos.6>.
- [38] Zhewei Yao, Reza Yazdani Aminabadi, Minjia Zhang, Xiaoxia Wu, Conglong Li, and Yuxiong He. Zeroquant: Efficient and affordable post-training quantization for large-scale transformers. *Advances in Neural Information Processing Systems*, 35:27168–27183, 2022. URL https://proceedings.neurips.cc/paper_files/paper/2022/file/adf7fa39d65e2983d724ff7da57f00ac-Paper-Conference.pdf.
- [39] Fanghua Ye, Yue Feng, and Emine Yilmaz. ASSIST: Towards label noise-robust dialogue state tracking. In Smaranda Muresan, Preslav Nakov, and Aline Villavicencio, editors, *Findings of the Association for Computational Linguistics: ACL 2022*, pages 2719–2731, Dublin, Ireland, May 2022. Association for Computational Linguistics. doi: 10.18653/v1/2022.findings-acl.214. URL <https://aclanthology.org/2022.findings-acl.214>.
- [40] Fanghua Ye, Jarana Manotumruksa, and Emine Yilmaz. MultiWOZ 2.4: A multi-domain task-oriented dialogue dataset with essential annotation corrections to improve state tracking evaluation. In Oliver Lemon, Dilek Hakkani-Tur, Junyi Jessy Li, Arash Ashrafzadeh, Daniel Hernández Garcia, Malihe Alikhani, David Vandyke, and Ondřej Dušek, editors, *Proceedings of the 23rd Annual Meeting of the Special Interest Group on Discourse and Dialogue*, pages 351–360, Edinburgh, UK, September 2022. Association for Computational Linguistics. doi: 10.18653/v1/2022.sigdial-1.34. URL <https://aclanthology.org/2022.sigdial-1.34>.
- [41] Xiaoju Ye. calflops: a flops and params calculate tool for neural networks in pytorch framework. 2023. URL <https://github.com/MrYxJ/calculate-flops.pytorch>.
- [42] Zihao Ye, Lequn Chen, Ruihang Lai, Yilong Zhao, Size Zheng, Junru Shao, Bohan Hou, Hongyi Jin, Yifei Zuo, Liangsheng Yin, Tianqi Chen, and Luis Ceze. Accelerating self-attentions for llm serving with flashinfer, February 2024. URL <https://flashinfer.ai/2024/02/02/introduce-flashinfer.html>.
- [43] Zihao Ye, Ruihang Lai, Bo-Ru Lu, Chien-Yu Lin, Size Zheng, Lequn Chen, Tianqi Chen, and Luis Ceze. Cascade inference: Memory bandwidth efficient shared prefix batch decoding, February 2024. URL <https://flashinfer.ai/2024/02/02/cascade-inference.html>.
- [44] Wen-wai Yim, Yujuan Fu, Asma Ben Abacha, Neal Snider, Thomas Lin, and Meliha Yetisgen. Aci-bench: a novel ambient clinical intelligence dataset for benchmarking automatic visit note generation. *Scientific Data*, 10(1):586, 2023. URL <https://www.nature.com/articles/s41597-023-02487-3.pdf>.
- [45] Ali Hadi Zadeh, Isak Edo, Omar Mohamed Awad, and Andreas Moshovos. Gobo: Quantizing attention-based nlp models for low latency and energy efficient inference. In *2020 53rd Annual IEEE/ACM International Symposium on Microarchitecture (MICRO)*, pages 811–824. IEEE, 2020. URL <https://microarch.org/micro53/papers/738300a811.pdf>.

- [46] Yusen Zhang, Ansong Ni, Ziming Mao, Chen Henry Wu, Chenguang Zhu, Budhaditya Deb, Ahmed Awadallah, Dragomir Radev, and Rui Zhang. Summⁿ: A multi-stage summarization framework for long input dialogues and documents. In Smaranda Muresan, Preslav Nakov, and Aline Villavicencio, editors, *Proceedings of the 60th Annual Meeting of the Association for Computational Linguistics (Volume 1: Long Papers)*, pages 1592–1604, Dublin, Ireland, May 2022. Association for Computational Linguistics. doi: 10.18653/v1/2022.acl-long.112. URL <https://aclanthology.org/2022.acl-long.112>.
- [47] Jeffrey Zhao, Raghav Gupta, Yuan Cao, Dian Yu, Mingqiu Wang, Harrison Lee, Abhinav Rastogi, Izhak Shafran, and Yonghui Wu. Description-driven task-oriented dialog modeling. *arXiv preprint arXiv:2201.08904*, 2022. URL <https://arxiv.org/abs/2201.08904>.
- [48] Yilong Zhao, Chien-Yu Lin, Kan Zhu, Zihao Ye, Lequn Chen, Size Zheng, Luis Ceze, Arvind Krishnamurthy, Tianqi Chen, and Baris Kasikci. Atom: Low-bit quantization for efficient and accurate llm serving. *arXiv preprint arXiv:2310.19102*, 2023. URL <https://arxiv.org/abs/2310.19102>.
- [49] Lianmin Zheng, Liangsheng Yin, Zhiqiang Xie, Jeff Huang, Chuyue Sun, Cody Hao Yu, Shiyi Cao, Christos Kozyrakis, Ion Stoica, Joseph E Gonzalez, et al. Efficiently programming large language models using sglang. *arXiv preprint arXiv:2312.07104*, 2023. URL <https://arxiv.org/abs/2312.07104>.
- [50] Sitong Zhou, Meliha Yetisgen, and Mari Ostendorf. Building blocks for complex tasks: Robust generative event extraction for radiology reports under domain shifts. In Tristan Naumann, Asma Ben Abacha, Steven Bethard, Kirk Roberts, and Anna Rumshisky, editors, *Proceedings of the 5th Clinical Natural Language Processing Workshop*, pages 344–357, Toronto, Canada, July 2023. Association for Computational Linguistics. doi: 10.18653/v1/2023.clinicalnlp-1.38. URL <https://aclanthology.org/2023.clinicalnlp-1.38>.

A Limitations

The types of tasks where our method is applicable are currently limited because we require decomposable tasks with a shared input document. The subtasking strategies in our datasets were designed by humans, e.g., according to structured output sections. Instead of using human-designed subtasking rules, a potential avenue for exploration is to allow a model to learn how to subtask, which can additionally make more tasks possible. While our subtasking experiments use only encoder-decoder models, our strategy of sharing an embedding and decomposing a task should work with decoder-only models, but experimental analysis is left to future work.

B Detailed Performance Analysis

Higher operational intensity bring more efficient matrix computation in modern accelerators such GPUs/TPUs. In this section, we detail the performance analysis and compare the operational intensity ratios of PiE and PiD. To simplify equations, we follow the previous work [30, 6, 1], using the inverse operational intensity (\mathcal{R}) to compare all modules. The lower inverse ratio indicates higher operational intensity, hence better performance.

We discuss memory access and number of floating-point operations of encoder’s self-attention, decoder’s self-attention and decoder’s cross-attention for PiE and PiD, respectively. We denote n_s , n_t and n_p as input length, output length and prompt length. U is number of prompts/subtasks. d is the joint dimension of all heads of key/query/value vectors.

We approximate the memory access and the number of operations based on the dominant terms in the self- and cross-attention and ignore the constant terms. For a single input, the memory access of the key or value tensors \mathbf{M} or \mathbf{N} are $n_s d$ and $n_t d$. The memory access of the projection matrices of key/query/value/output tensors W^K, W^Q, W^V, W^O is d^2 . As described in Shazeer [30], the number of operations in both attention mechanisms is dominated by the matrix projections which are used to obtain projected query/key/value/output tensors ($\mathbf{Q}/\mathbf{K}/\mathbf{V}/\mathbf{O}$); thus, the number of operations is approximated as $n_s d^2$ or $n_t d^2$.

B.1 Encoder’s self-attention

The inverse operational intensity of PiE’s encoder can be written as follows,

$$\begin{aligned} \mathcal{R}_{\text{PiE}}^{\text{Enc-self}} &= \frac{\underbrace{Ub(n_s + n_p)d + d^2}_{\text{memory access}}}{\underbrace{Ub(n_s + n_p)d^2}_{\text{\# operations}}} \\ &= \frac{1}{d} + \frac{1}{Ub(n_s + n_p)}, \end{aligned}$$

where PiE’s encoder individually encodes U prompts (Z_1, \dots, Z_U) with input \mathcal{X} . $\mathcal{R}_{\text{PiE}}^{\text{Enc-self}}$ is a low ratio given the fact that n_s is usually an hundred or a thousand tokens and d is usually near a thousand.

Different from PiE’s encoder, PiD’s encoder only encodes input \mathcal{X} and leaves prompts in the decoder. Thus, the memory access is lower than PiE by a factor of U and only the input length n_s is considered. More formally the inverse operational intensity of PiD’s encoder is denoted as

$$\begin{aligned} \mathcal{R}_{\text{PiD}}^{\text{Enc-self}} &= \frac{\underbrace{bn_s d + d^2}_{\text{memory access}}}{\underbrace{bn_s d^2}_{\text{\# operations}}} \\ &= \frac{1}{d} + \frac{1}{bn_s}. \end{aligned}$$

Again, n_s and d is around a thousand, resulting in $\mathcal{R}_{\text{PiD}}^{\text{Enc-self}}$ is also a low ratio. Compared to PiE, PiD requires fewer number of operations, saving more memory usage and enabling faster computation.

B.2 Decoder’s self-attention

In PiE, prompts are encoded in the encoder, the decoder only accounts for generating target tokens. The inverse operational intensity of PiE encoder’s self-attention is denoted as

$$\begin{aligned}\mathcal{R}_{\text{PiE}}^{\text{Dec-self}} &= \frac{\underbrace{Ubn_t^2d + n_td^2}_{\text{memory access}}}{\underbrace{Ubn_td^2}_{\text{\# operations}}} \\ &= \underbrace{\frac{n_t}{d}}_{\text{dominant term}} + \frac{1}{Ub},\end{aligned}$$

where $\frac{n_t}{d}$ is the dominant term that causes the issue of slower incremental decoding.

PiD’s decoder encodes prompts and incrementally generates output tokens. We decouple the analysis of encoding prompts and generating output tokens since the prompts are all given whereas the output tokens are incrementally decoded. The decoder just need to encode the prompts once; as a result, the ratio can be written as

$$\begin{aligned}\mathcal{R}_{\text{PiD}}^{\text{Dec-self,prompt}} &= \frac{\underbrace{Ubn_p d + d^2}_{\text{memory access}}}{\underbrace{Ubn_p d^2}_{\text{\# operations}}} \\ &= \frac{1}{d} + \frac{1}{Ubn_p}\end{aligned}$$

Obviously, the $\mathcal{R}_{\text{PiD}}^{\text{Dec-self,prompt}}$ is a low ratio; thus the encoding prompts in the decoder part is efficient. In addition to encoding prompts, PiD’s decoder needs to generate output tokens. The ratio $\mathcal{R}_{\text{PiD}}^{\text{Dec-self,output}}$ is the same as $\mathcal{R}_{\text{PiE}}^{\text{Dec-self}}$.

B.3 Decoder’s cross-attention

In transformer architecture, the decoder’s cross-attention is the key issue that cause the computation inefficiency since the inference is incremental and cross-attention needs to read the huge chunk of key and value cached tensors from the encoder. The inverse operational intensity of PiE decoder’s cross-attention can be denoted as follows,

$$\begin{aligned}\mathcal{R}_{\text{PiE}}^{\text{Dec-cross}} &= \frac{\overbrace{Ub(n_s + n_p)n_td + Ubn_td + n_td^2}^{\text{memory access}}}{\underbrace{Ubn_td^2}_{\text{\# operations}}} \\ &= \underbrace{\frac{n_s + n_p + 1}{d}}_{\text{dominant term}} + \frac{1}{Ub},\end{aligned}$$

where the prompts are encoded with the input in the encoder; hence the length of cached tensors is $n_s + n_p$. The dominant term results in a serious bottleneck especially when long input n_s is fed into the model.

Similar to the PiD decoder’s self-attention, we consider the cross-attention on prompts and output separately. The ratio for encoding prompts is as follows,

$$\begin{aligned}\mathcal{R}_{\text{PiD}}^{\text{Dec-cross,prompt}} &= \frac{\overbrace{bn_s d + Ubn_p d + d^2}^{\text{memory access}}}{\underbrace{Ubn_p d^2}_{\text{\# operations}}} \\ &= \underbrace{\frac{1}{d} \cdot \left(\frac{n_s}{Un_p} + 1 \right)}_{\text{dominant term}} + \frac{1}{Ubn_p}.\end{aligned}$$

In the dominant term, the input length n_s is divided by the factor of Un_p .

On the other hand, the ratio of decoding output tokens is

$$\mathcal{R}_{\text{PiD}}^{\text{Dec-cross,output}} = \frac{\overbrace{bn_s n_t d + Ubn_t d + n_t d^2}^{\text{memory access}}}{\underbrace{Ubn_t d^2}_{\text{\# operations}}} = \frac{1}{d} \cdot \underbrace{\left(\frac{n_s}{U} + 1\right)}_{\text{dominant term}} + \frac{1}{Ub}.$$

Similarly, in the dominant term, the input length n_s is divided by the factor of U . Overall, in PiD decoder’s cross-attention, the dominant term of the incremental decoding is reduced by a factor of U or Un_p since PiD shares the same input key and value cached tensors and broadcast the matrix operations while performing the cross-attention.

Table 10: The PiD-T5 hyperparameters used in the training and testing.

	MultiWoZ 2.4		ACI-Bench		RadQA	
	PiD-T5 _{base}	PiD-T5 _{large}	PiD-T5 _{base}	PiD-T5 _{large}	PiD-T5 _{base}	PiD-T5 _{large}
Batch size	4	1	1	2	4	2
Gradient accumulation	64	32	16	16	16	32
Effective batch size	64	64	32	32	64	64
# epochs	6	4	100	100	50	15
Max input length	1024	1024	3072	3072	1024	1024
Max output length	24	24	1024	1024	92	92
Max prompt length	8	8	6	6	36	36
# outputs	30	30	4	4	2-6	2-6
# beams	1	1	4	4	1	1

C Training Details

Table 10 presents the hyperparameters selected for the training and testing phases. We executed a search for the optimal learning rate across the following set of values: $\{5 \times 10^{-4}, 3 \times 10^{-4}, 1 \times 10^{-4}, 7 \times 10^{-5}, 5 \times 10^{-5}, 3 \times 10^{-5}\}$ to identify the most effective learning rate for each dataset. All reported values represent the medians of three different random runs. The remaining hyperparameters not mentioned in Table 10 are set to the default values provided by the HuggingFace Transformers package. Training time varies because of dataset size, model size, model configuration and training procedure. Our experiments, which utilize T5_{base} as the primary framework, are carried out using a single NVIDIA A40. Training T5_{base} and PiD-T5_{base} on the MultiWoZ 2.4 dataset typically requires approximately 5 GPU hours, whereas it takes around 46 GPU hours for PiE-T5_{base}. In the case of ACI-Bench, where the dataset is relatively small, T5_{base}, PiE-T5_{base}, and PiD-T5_{base} require roughly 4 GPU hours each. On the other hand, for RadQA, PiE-T5_{base} takes 2 hours, while PiD-T5_{base} requires 3 GPU hours. When switching to T5_{large}, the required GPU training time increases by a factor of 2 to 3 times compared to the T5_{base} models.

We use t5-base⁴ and t5-large⁵ checkpoints downloaded from HuggingFace as initialization for MultiWoZ 2.4 and ACI-Bench. For RadQA, we follow the previous work [18] to use pretrained clinical T5 models.⁶

D Datasets

In terms of data preprocessing, we follow the previous works [39, 44, 18] to process MultiWoZ 2.4, ACI-Bench and RadQA, respectively. The dataset statistics are shown in Table 11.

⁴<https://huggingface.co/google-t5/t5-base>

⁵<https://huggingface.co/google-t5/t5-large>

⁶<https://physionet.org/content/clinical-t5/1.0.0/>

Table 11: Statistics are calculated on the each full data set. Input and output lengths are calculated based on Huggingface T5 tokenizer.

	MultiWoZ 2.4	ACI-Bench	RadQA
Data	Task oriented	Medical	Medical
Input type	Dialogue	Dialogue	Document
Task	Dialog state tracking	Summarization	Question Answering
# examples	9887	207	6148
Input length	$289_{\pm 108}$	$1725_{\pm 511}$	$137_{\pm 157}$
Output length	$56_{\pm 26}$	$693_{\pm 200}$	$28_{\pm 49}$
Prompt type	Fixed	Fixed	Free-form
# prompts	30 slots or 5 domains	4 sections	–

E License of Artifacts

The licensing for the code from HuggingFace’s transformers [37] falls under the Apache License, Version 2.0. PyTorch [26] is open-source software released under the modified BSD license. Meanwhile, the calflops [41] code is protected under the MIT License. Detailed conditions for utilizing our artifacts will be provided within the package we distribute.